Robotica (2014) volume 32, pp. 1245–1263. © Cambridge University Press 2014
doi:10.1017/S0263574714001453

A novel robotic knee device with stance control and its kinematic weight optimization for rehabilitation

Sanghun Pyo†, Junwon Yoon†* and Min-Kyun Oh‡

†*Intelligent Robots and Systems Lab, School of Mechanical and Aerospace Engineering and ReCAPT, Gyeongsang National University, Jinju, South Korea*
‡*Department of Rehabilitation Medicine, Gyeongsang National University Hospital, Jinju, South Korea*

(Accepted May 12, 2014. First published online: June 13, 2014)

SUMMARY
It is important to develop a robotic orthosis or exoskeleton that can provide back-drivable and good assistive performances with lightweight structures for overground gait rehabilitation of stroke patients. In this paper, we describe a robotic knee device with a five-bar linkage to allow low-impedance voluntary knee motion within a specified rotation range during the swing phase, and to assist knee extension during the stance phase. The device can provide free motion through the five-bar linkage with 2-degree-of-freedom (DOF) actuation via the patient's shank using a linear actuator, and can assist knee extension at any controlled knee angle while bearing weight via a geared five-bar linkage with 1 DOF actuation of the linear actuator. The kinematic transition between the two modes can be implemented by contact with a circular structure and a linear link, and the resultant range of motion can be determined by the linear actuator. The kinematic weight of the device was optimized using the simple genetic algorithm to reduce the mass. The optimization cost function was based on the sum of the total link lengths and the actuator power. The optimization results reduced the total link length and motor power by 47% and 43%, respectively, compared to the initial design. We expect that the device will facilitate rehabilitation of stroke patients by allowing safe and free overground walking while providing support for stumbling.

KEYWORDS: Exoskeletons; Human biomechanics; Design; Man-machine systems; Novel applications of robotics.

1. Introduction

A stroke, or cerebrovascular accident (CVA), is the rapid loss of brain function due to a disturbance in the blood supply to the brain.[1] As a consequence, stroke patients may lose some body function, which may severely impact their walking gait. If spontaneous recovery does not occur, the patient will require rehabilitation.[2,3] Active orthoses or exoskeletons have been proposed to support gait rehabilitation for patients suffering from paralysis as a consequence of stroke or other neurological diseases.[4]

Reciprocating gait orthosis (RGO) is commonly used to support stroke patients.[5] RGO can support a patient's weight during the stance phase, helping patients with a paretic limb to walk unaided. However, such devices can cause asymmetry of the gait because of the irregular and sudden impulsive supports. Kobetic[6] proposed an active knee orthosis system with exoskeletal bracing and multichannel functional electrical stimulation. The knee mechanism consisted of electro-mechanical joint locks to provide upright stability only during the stance phase. However, the simple locking mechanism of the electronic switching did not provide active assistance to the knee joint.

Jin[7] designed a prosthetic knee device based on optimization of a six-bar linkage to generate trajectories that better approximate a normal gait. "Roboknee"[8] is a robotic exoskeleton based on a four-bar linkage and includes an active slide-crank with a series elastic actuator. Colombo[9] developed

* Corresponding author. E-mail: jwyoon@gnu.ac.kr

https://doi.org/10.1017/S0263574714001453 Published online by Cambridge University Press

Fig. 1. (Colour online) The prototype of robotic knee device with a five-bar linkage for stance control.

a rehabilitation system for a treadmill, where the mechanism of the knee joint consisted of a simple four-bar linkage. Mefoued[10] suggested a 1-degree-of-freedom (DOF) knee actuation system with a chain drive controlled by a high-order sliding mode controller. Nikitczuk[11] developed a knee brace consisting of a planetary gear mechanism and variable damper component. Belforte[12] used a direct drive based on a chain mechanism with a pneumatic cylinder for knee joint support.

However, even though it is possible to augment knee support using existing 1-DOF robotic knee systems,[7–13] it is difficult to apply the existing systems directly to patients with neurologic diseases. Existing 1-DOF systems do not simultaneously satisfy the requirements of sufficient knee torque to support a patient's weight during the stance phase while providing backdrivability and low-weight actuators suitable for wearable systems. To overcome these problems, Veneman[14] designed an actuation system for knee joints that consisted of a servomotor, a flexible Bowden cable transmission, and a force feedback loop based on a series elastic element to supply torque to the knee joint. His actuation system aimed to produce an impedance-controlled gait rehabilitation robot for treadmill training. Similarly, Ackermann[15] and Sulzer[16] developed a powered knee orthosis that can provide knee flexion torque in the swing phase to compensate for the gait abnormality known as stiff-knee gait (SKG). But even though both knee actuation systems produce high torque with small impedance, they are limited to treadmill-training applications since the actuators must be located on a fixed base.

Recent clinical studies[17] of gait rehabilitation have shown that treadmill gait training is not as effective as gait training through overground walking. In addition, reduced assistance may increase the effectiveness of training resulting in greater flexibility of motion.[18] Therefore, it is important to develop gait rehabilitation systems that can provide high impedance for safe support as well as low impedance for free voluntary motions while allowing overground training. The recently introduced stance-control knee–ankle–foot orthoses (SCKAFOs)[19] allow wearers to flex their knee when swinging the leg forward while preventing knee flexion while bearing weight. However, existing SCKAFOs cannot provide powered knee extension assistance at any desired knee angle, which is important for adapting to different walking conditions, such as slopes or stairs, or handling unexpected conditions such as stumbling.

In this paper, we describe a robotic knee device, shown in Fig. 1, that can provide free knee motion during the swing phase and assist knee extension during the stance phase at any desired knee angle. Voluntary motions with minimum impedance can be achieved via a 2-DOF five-bar linkage and a linear actuator. The proposed five-bar linkage in this paper is a novel kinematic mechanism with one prismatic joint and thee revolute joints, which can allow a wearer to move freely the knee joint with low impedance independent of an actuator, while the knee joint with the existing four-bar and six-bar linkages[7–10,13] were directly connected to an actuator without permission for free movements of the knee joint. In addition, a 1-DOF geared five-bar linkage with a linear actuator can provide the necessary impedance for weight support. These functionalities can be implemented via a kinematic transition through the contact conditions between the 2-DOF five-bar linkage and the 1-DOF geared five-bar linkage. Such an active knee device requires additional linkages compared with a simple four-bar mechanism. To maximize the benefit of the proposed device, it is necessary to minimize its total mass while maintaining the necessary actuator performance for the required torques and

https://doi.org/10.1017/S0263574714001453 Published online by Cambridge University Press

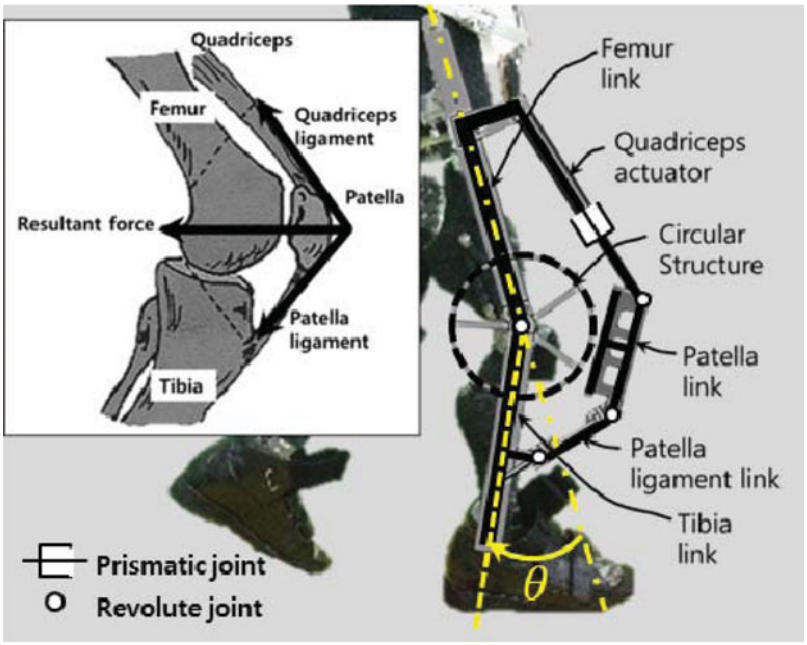

Fig. 2. (Colour online) Concept of our knee orthosis.

angular velocities during the gait cycle. For this purpose, we used a simple genetic algorithm (SGA) to minimize the sum of the total link lengths and the motor power by reducing the mass of the device. This kinematic optimization scheme resulted in a significant reduction in the total mass of the system, and hence enhanced its portability compared to existing four-bar mechanisms.

The remainder of the paper is organized as follows. We introduce the basic concepts of the system in Section 2 and describe kinematic analyses of the device in Section 3. We provide an optimal design scheme to reduce the mass of the system in Section 4. We discuss our results in Section 5, and present our conclusions and directions for future work in Section 6.

2. Design Concept for Portable Stance Control

In the biomechanics of the knee, the moment required to support the weight of the human body is generated primarily by contraction of the quadriceps. When this occurs, a reaction force is produced by the patella ligament, which results in a moment at the knee.[20,21] The conceptual design of an active knee orthosis must be realized by taking into account the biomechanics of the knee joint. This concept is illustrated in Fig. 2. Since the mechanical functioning of the quadriceps muscle resembles linear movements of an actuator, the proposed knee device was designed so that the angle between the femur and tibia links can be determined from the displacement of a linear actuator.

The design primarily aims to support the patient's lower limb movements during the stance phase, especially when the quadriceps muscle cannot provide the necessary knee moments to support the body weight. When a patient can walk by himself or herself, the actuator operates in free mode with minimum impedance due to friction at the revolute joints. For this purpose, the maximum allowable motion ranges of the knee joint can be determined individually for each patient, and the corresponding displacement of the quadriceps actuator can be calculated to satisfy the specified motion range based on the kinematics of the device, as described in Section 3.

Within the specified range of motion, the wearer can move their knee joint freely with the 2-DOF five-bar mechanism since the patella link does not make contact with the circular structure, as shown in Fig. 3. When the patient loses gait stability and the knee angle exceeds an allowable range of motion during the stance phase, the five-bar linkage will be changed to a 1-DOF geared five-bar linkage due to mechanical contact between the patella link and the circular structure (see Section 3.1 for a detailed description of the geared five-bar linkage). After contact, the knee joint angle and the shank of the lower limb are controlled by the quadriceps linear actuator, which can provide mechanical assistance.

https://doi.org/10.1017/S0263574714001453 Published online by Cambridge University Press

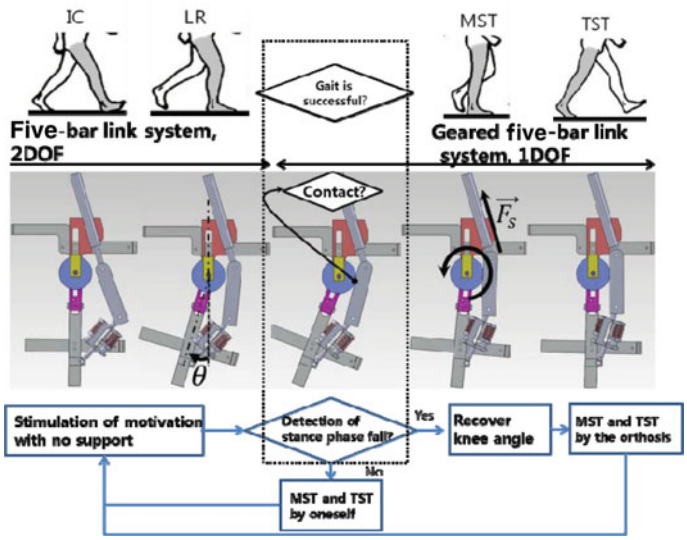

Fig. 3. (Colour online) Transition from the 2-DOF five-bar linkage to the 1-DOF geared five-bar linkage due to mechanical contact between the patella link and the circular structure.

Hence, this active knee device with contact and non-contact modes can provide additional supportive motions as well as voluntary unrestricted motions for better gait therapy.

Although the contact mechanism is mechanically generated by the motion of the wearer, the contact condition can also be detected electrically by measuring the currents of the quadriceps actuator with a linear direct current (DC) motor. This contact condition can be used to evaluate whether the patient can successfully walk within an adequate range of motion of the knee. When required, the quadriceps actuator can provide control assistance through the geared five-bar linkage. However, if the contact condition from the quadriceps actuator is not detected, the device does not provide any assistance, which means that the patient can support his own weight.

3. Kinematic Analysis

3.1. Orthosis

Figure 4 shows a kinematic model of the knee device during non-contact conditions. The linkages can be classified into bionic-based links and structural links. The length of the structural links are as follows: l_{cqa} is the length of the connecting linkage to the quadriceps actuator, l_{cptl} is the length of the connecting linkage to the patella ligament link, r is the radius of the circular structure, and w is the width of the patella link.

For the bionic-based link shown in Fig. 4, S is the displacement of the quadriceps actuator, l_{fm} is the length of the femur link, l_{tb} is the length of the tibia link, l_{ptl} is the length of the patella ligament link, and l_{pt} is the length of the patella link. The parameter λ is the angle between the l_{bar} linkage and the femur length, which is fixed, and θ^* is the angle of the knee joint.

The number of DOFs of the knee orthosis can be determined from the mechanical contact between the patella link and the circular structure, as described in Section 2. To analyze the kinematic behavior of the knee device, the Grübler–Kutzbach criterion was used, i.e.,

$$m = 3(n-1) - 2j_1 - j_2, \tag{1}$$

Where m is the number of DOFs, n is the number of links, j_1 is the number of 1-DOF (full) joints, and j_2 is the number of 2-DOF (half) joints.

In the non-contact condition, the mechanism is composed of five links, four revolute joints, and one prismatic joint, so $m = 2$ (because $j_1 = 5$, $j_2 = 0$, and $n = 5$). The wearer can move their knee joint freely and independently because the quadriceps actuator does not have an effect on the knee joint. When there is contact between the circular structure and the patella link, the structure becomes

https://doi.org/10.1017/S0263574714001453 Published online by Cambridge University Press

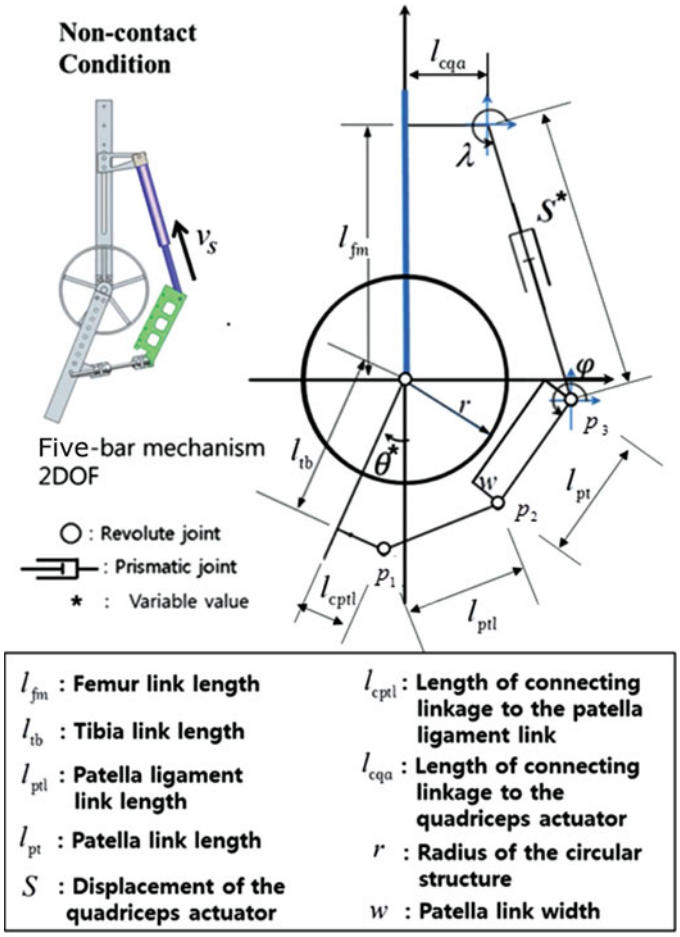

Fig. 4. (Colour online) The knee device under non-contact conditions, showing the link labels and the angles between links.

a geared five-bar linkage, as shown in Fig. 5. Contact between the patella link and the circular structure means that the joint can be considered as a half joint with 2 DOFs: rolling and sliding. The line that extends from the center of the circular structure to the contact point on the patella link is perpendicular to the direction of the sliding motion of the joint. In addition, it should be noted that the contact condition can transfer unidirectional motion for knee extension. Since the tibia link and the circular structure are rigidly connected, knee extension can be controlled by the quadriceps actuator. Thus, in the contact condition, the device is composed of four revolute joints and one prismatic joint, as well as one half joint (sliding–rolling joint). From Eq. (1), the number of DOFs becomes $m = 1$ (because $j_1 = 5, j_2 = 1$, and $n = 6$).

Figure 5 shows the knee orthosis under contact conditions. Let v_s be the velocity of the quadriceps linear actuator, F_s be the force, and T be the resultant torque. Angle θ_c between the tibia link and the femur link may be controlled by the linear actuator under contact conditions. The following relationship describes the geared five-bar kinematics of the device:

$$\theta_c = f(S)(0^\circ \leq \theta_c \leq 50^\circ), \tag{2}$$

where S is the displacement of the quadriceps actuator. To solve Eq. (2), the position vectors of each revolute joint described by $\overrightarrow{p_n}$ can be expressed as

$$\begin{aligned} \overrightarrow{p_1} &= (-l_{\text{tb}} \sin\theta_c + l_{\text{cptl}} \cos\theta_c)\vec{i} + (-l_{\text{tb}} \cos\theta_c - l_{\text{cptl}} \sin\theta_c)\vec{j}, \\ \overrightarrow{p_3} &= (l_{\text{cqa}} + S\cos\lambda)\vec{i} + (l_{\text{fm}} + S\sin\lambda)\vec{j}, \end{aligned} \tag{3}$$

https://doi.org/10.1017/S0263574714001453 Published online by Cambridge University Press

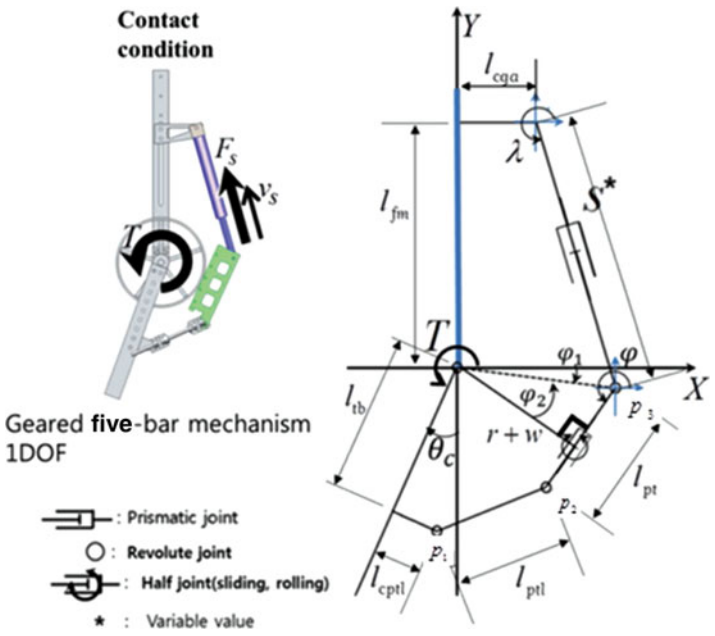

Fig. 5. (Colour online) Geared five-bar mechanism under contact conditions.

where angles φ_1 and φ_2 shown in Fig. 5 can be expressed as

$$\varphi_1 = \tan^{-1}\left(\frac{l_{\text{fm}} + S\sin\lambda}{l_{\text{cpa}} + S\cos\lambda}\right) \tag{4}$$

and

$$\varphi_2 = \cos^{-1}\left(\frac{(r+w)}{\sqrt{\left(l_{\text{cqa}} + S\cos\lambda\right)^2 + (l_{\text{fm}} + S\sin\lambda)^2}}\right). \tag{5}$$

The angle φ is given by

$$\varphi = \frac{3}{2}\pi - \varphi_2 + \varphi_1. \tag{6}$$

The position vector $\overrightarrow{p_2}$ can be expressed as

$$\overrightarrow{p_2} = \left(l_{\text{cqa}} + S\cos\lambda + l_{\text{pt}}\cos\varphi\right)\vec{i} + \left(l_{\text{fm}} + S\sin\lambda + l_{\text{pt}}\sin\varphi\right)\vec{j}, \tag{7}$$

and the kinematic relationship between $\overrightarrow{p_1}$ and $\overrightarrow{p_2}$ is constrained by length of patella link, l_{ptl}. The relationship between the displacement of the quadriceps actuator, S, and the angle of tibia link, θ_c, can be defined as

$$\begin{aligned} l_{\text{ptl}}^2 = {} & \left(l_{\text{cqa}} + S\cos\lambda - l_{\text{cptl}}\cos\theta_c + l_{\text{cptl}}\cos\varphi + l_{\text{tb}}\sin\theta_c\right)^2 \\ & + \left(l_{\text{fm}} + l_{\text{tb}}\cos\theta_c + S\sin\lambda + l_{\text{cptl}}\sin\theta_c + l_{\text{pt}}\sin\varphi\right)^2. \end{aligned} \tag{8}$$

Using Eqs. (8) and (2) the relationship between the displacement of the quadriceps actuator and θ_c can be calculated as shown in Fig. 6, where the parameters describing the linkages are listed in Table I. The variable range indicated by θ^*, as shown in Fig. 6, represents the freely moving 2-DOF five-bar linkage. As the knee angle reaches the critical angle, the motion becomes that of the 1-DOF geared five-bar linkage. The displacement of the quadriceps actuator can determine how much of the range of motion of the knee joint is allowed to move freely. This is one of the major benefits

https://doi.org/10.1017/S0263574714001453 Published online by Cambridge University Press

Table I. Example set of initial parameters for the robotic knee device, where $\lambda = 4.9916$ rad.

l_{tb}	248 mm	w	56 mm
l_{cptl}	65 mm	l_{pt}	217 mm
l_{cqa}	110 mm	l_{ptl}	175.87 mm
r	140 mm	l_{fm}	419 mm

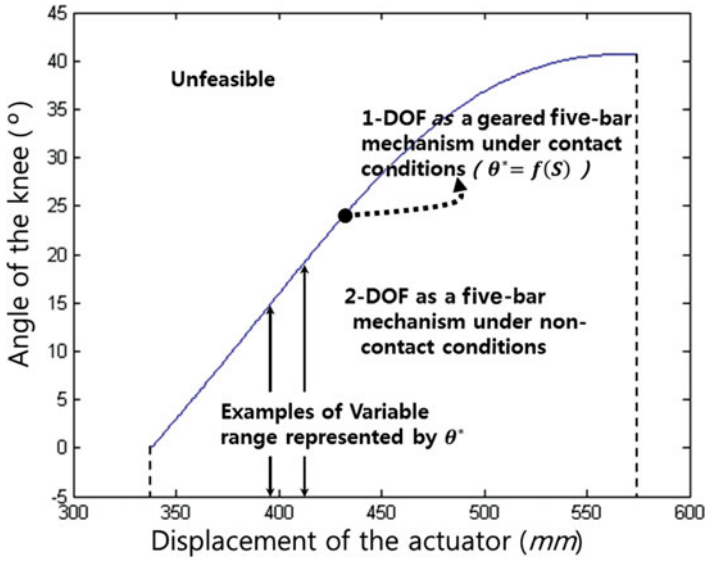

Fig. 6. (Colour online) Relationship between the quadriceps actuator and knee angle.

of this mechanism: the knee angle can be automatically locked by adjusting the displacement of the quadriceps actuator to prevent the knee from buckling due to the patient's weight.

3.2. Force and velocity

It is necessary to define the relationship between the force of the actuator and the resultant torque at the knee joint for the geared five-bar linkage under contact conditions. This torque can be used to assist the stance stability of the patient. The force and torque relationship can be defined using the free-body diagram shown in Fig. 7. The contact position, (x_c, y_c), defined by the circular structure and the patella link, can be determined using the geometrical relationships of a line and a circle. The term $\overrightarrow{C_r}$ shown in Fig. 7 is the reaction force from the circular structure to the patella link at the contact point. The coordinates of the contact point can be defined by the following two equations:

$$\left(x_c + w\cos\left(\varphi - {}^{\pi}/_{2}\right)\right)\tan\left(\varphi - {}^{\pi}/_{2}\right) - \left(y_c + w\sin\left(\varphi - {}^{\pi}/_{2}\right)\right) = 0 \tag{9}$$

and

$$-\frac{x_c + w\cos\left(\varphi - {}^{\pi}/_{2}\right)}{\left(\tan\left(\varphi - {}^{\pi}/_{2}\right)\right)} - \left(y_c + w\sin\left(\varphi - {}^{\pi}/_{2}\right)\right) = -l_{fm} - S\sin\lambda - \left(\frac{l_{cqa} + S\cos\lambda}{\tan\left(\varphi - {}^{\pi}/_{2}\right)}\right). \tag{10}$$

If (x_c, y_c) is re-defined using $\overrightarrow{C_p}$, the force relationship in Fig. 7 can be expressed by

$$-F_{p_2x} + R\cos\left(\varphi + {}^{\pi}/_{2}\right) = -F_s\cos\left(\lambda - \pi\right), \tag{11}$$

$$-F_{p_2y} + R\sin\left(\varphi + {}^{\pi}/_{2}\right) = -F_s\sin\left(\lambda - \pi\right), \tag{12}$$

and

$$\overrightarrow{p_2C_p} \times \overrightarrow{C_r} + \overrightarrow{p_2p_3} \times \overrightarrow{F_s} = 0. \tag{13}$$

https://doi.org/10.1017/S0263574714001453 Published online by Cambridge University Press

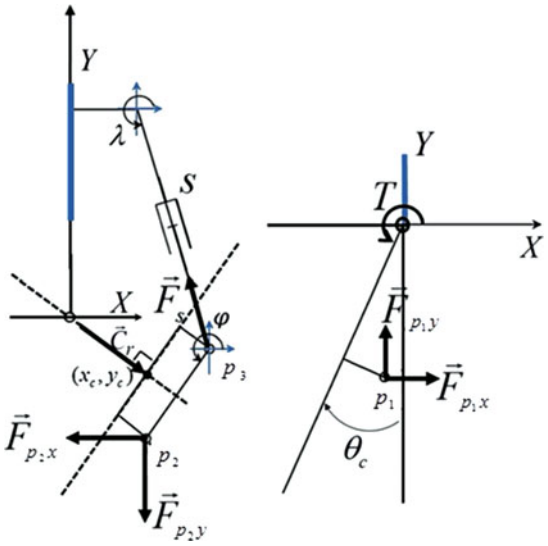

Fig. 7. (Colour online) Free body diagram of the knee orthosis.

Using these relationships, we arrive at

$$C_r\,(x_c - p_{2x})\sin\left(\varphi + {}^{\pi}/_{2}\right) - C_r\left(y_c - p_{2y}\right)\cos\left(\varphi + {}^{\pi}/_{2}\right) = (p_{3y} - p_{2y})F_s\cos(\lambda - \pi) - (p_{3x} - p_{2x})F_s\sin(\lambda - \pi)\,. \tag{14}$$

If F_s is given, the diagram shown in Fig. 7 can be described using Eqs. (11), (12), and (14). The moment $\overrightarrow{\mathrm{T}}$ generated by force $\overrightarrow{\mathrm{F}_{\mathrm{s}}}$ from the quadriceps actuator can be calculated from

$$\overrightarrow{F_{p_1}} = -\overrightarrow{F_{p_2}}, \tag{15}$$

and the moment $\overrightarrow{\mathrm{T}}$ can be expressed as

$$\overrightarrow{T} = \overrightarrow{p_1} \times \overrightarrow{F_{p_1}}, \tag{16}$$

which can be expressed in terms of the link lengths, i.e.,

$$T = F_{p_1y}(-l_{\mathrm{tb}}\sin\theta + l_{\mathrm{cptl}}\cos\theta) - F_{p_1x}(-l_{\mathrm{tb}}\cos\theta + l_{\mathrm{cptl}}\sin\theta). \tag{17}$$

Since the maximum range of knee angles in a normal gait pattern during the stance phase is less than 20°, [20] we can determine the force of the quadriceps actuator required to realize the necessary torque to support a patient during the stance phase in that angle range. Additionally, the angular velocity of the tibia link controlled by the quadriceps actuator can also be obtained by using Eq. (8), i.e.,

$$\dot{\theta} = \frac{\partial\theta_c}{\partial s}\cdot\frac{\mathrm{d}S}{\mathrm{d}t}. \tag{18}$$

4. Kinematic Optimization for Light Weight

The knee device described here requires more linkages than existing systems, which use a four-bar linkage,[7,9] and contains an additional circular structure to generate the contact condition. It is desirable to reduce the total length of the linkages of the knee device to reduce the total mass of the device. In addition, the appropriate actuator power should be determined to provide the necessary torque and angular velocity required for support. In this section, an optimization scheme is described for the link lengths and motor power.

https://doi.org/10.1017/S0263574714001453 Published online by Cambridge University Press

Table II. Parameters used in the SGA optimization.

Population	100
Maximum number of generations	50
Crossover chance, P_c	0.85
Mutation chance, P_m	0.05

Table III. Boundaries of the design parameters vector, Q.

Variables range of Q and its initial values							
l_{tb} (248 mm)		l_{cptl} (65 mm)		l_{cqa} (110 mm)		l_{pt} (217 mm)	
$q^{(L)}$	$q^{(U)}$	$q^{(L)}$	$q^{(U)}$	$q^{(L)}$	$q^{(U)}$	$q^{(L)}$	$q^{(U)}$
10	350	10	400	10	400	10	400
l_{ptl} (175.87 mm)		l_{fm} (419 mm)		$\dot{S}$ (320 mm/s)		F_s(150 N)	
$q^{(L)}$	$q^{(U)}$	$q^{(L)}$	$q^{(U)}$	$q^{(L)}$	$q^{(U)}$	$q^{(L)}$	$q^{(U)}$
10	400	100	410	10	300	100	999

Note: $\lambda = 4.9916$ rad.

4.1. Genetic algorithm

Since the performance of the knee device is highly non-linear (due to the many linkages), it is not straightforward to determine the optimal kinematic parameters. Thus, Holland's SGA[22] was used to determine the optimal design. The SGA algorithm has been successfully applied to design optimization of a 6-DOF haptic device,[23] as well as to assembly algorithms with path planning for active haptic guidance.[24,25]

The variables in the optimization are the linkage lengths l_{fm}, l_{tb}, l_{cptl}, l_{ptl}, and l_{pt}; $r + w$; S; and the actuator specifications F_s and $\dot{S}$. Table II shows the parameters used in the genetic algorithm.

4.2. Cost function

The cost function for the optimization can be defined as

$$\min f = \left(\frac{\sum L_{\text{gen}}}{\sum L_{\text{initial}}} + \frac{F_S}{F_{S_{\text{initial}}}} \cdot \frac{\dot{S}}{\dot{S}_{\text{initial}}} + SP + GP \right), \tag{19}$$

where L_{initial} represents the initial set of all linkage lengths listed in Table I, L_{gen} is the union set composed of linkages created by the SGA (L_{al}) and the initial posture condition (S, R), and F_S and $\dot{S}$ are the chromosomes related to the power of the quadriceps actuator. The first term of Eq. (19) aims to reduce the total linkage length and the second term is related to minimize the power of the quadriceps actuator. The specification penalty, SP, and the geometrical penalty, GP, can be defined as follows:

$$\begin{gathered} \text{Penalty} = \text{SP} + \text{GP} = \sum_{i=1}^{3} r_i \left(g_+^{(i)} \right) + \sum_{i=4}^{10} r_i \left(g_+^{(i)} \right), \\ g_+^{(i)} = \max(0, g^{(i)}). \end{gathered} \tag{20}$$

SP is related to the required performance of the knee device and GP deals with the kinematic feasibility to avoid singular configurations.

4.3. Kinematic feasibility, boundary conditions, and constraints

The range of the linkage lengths, initial posture, and constraints of the mechanism configuration must be considered to obtain feasible optimizations.

4.3.1. Boundary of the linkage lengths (side constraint). The length constraints of the design variable vector, Q, to adjust the system boundaries are listed in Table III. Q must satisfy the following

https://doi.org/10.1017/S0263574714001453 Published online by Cambridge University Press

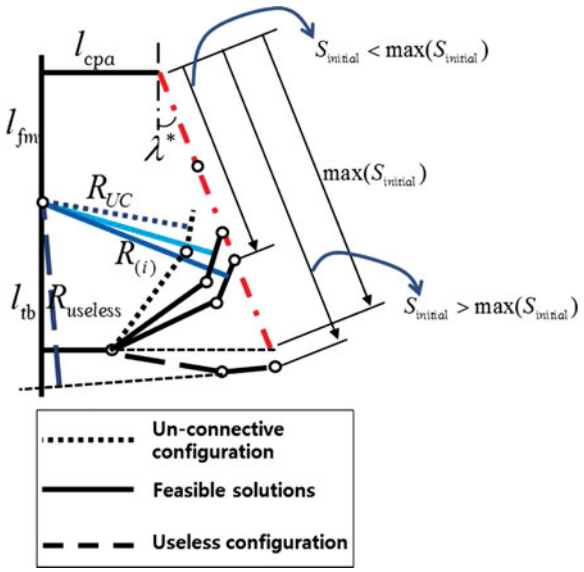

Fig. 8. (Colour online) Sets of feasible initial posture and infeasible sets within the boundary condition of S_{initial}.

relationships:

$$\mathrm{Q} = \{\mathrm{Q}|q^{(L)} \le q \le q^{(U)}\}\mathrm{Q} = L_{\text{al}} \cup \{\dot{S},\, F_S\}L_{\text{al}} = \{l_{\text{tb}}, l_{\text{cptl}}, l_{\text{cqa}}, l_{\text{pt}}, l_{\text{ptl}}, l_{\text{fm}}\}. \tag{21}$$

The maximum ranges of the linkages were selected based on typical human body size. The actuator's specifications ($\dot{S}$, F_S) were a power of less than 300 W, which follows from 300 mm/s $\times$ 999 N and is almost the same as was used for Roboknee's actuator speed (280 mm/s).[9]

4.3.2. Initial posture determination algorithm. Under contact conditions, the length $r + w$ must be considered as a kinematic constraint for a feasible design because the $r + w$ link (or R-link) is closely related to the initial displacement $S_{initial}$ of the quadriceps actuator. The length of the R-link and initial displacement of the quadriceps actuator, L_{al}, can be found using an incremental numeric method based on Eq. (8) when $\theta_c = 0$, i.e.,

$$R_{(i)} = f\left(S_{\text{initial}_{(i)}}, L_{\text{al}}\right), \quad \text{where}\, \theta_c = 0^\circ, \quad i = 1,\, 2, \ldots\ . \tag{22}$$

To obtain feasible sets of solutions and to avoid those sets that may result in useless configurations as shown in Fig. 8, the maximum value of the search range about S_{initial} can be determined as follows:

$$\max\left(S_{\text{initial}_{(i)}}\right) < {(l_{\text{fm}} + l_{\text{tb}})}/{\cos\lambda^*}. \tag{23}$$

Among the sets $[\{\text{set}\}_{(i)}]$ ensuring kinematic feasibility, the set $\{s_{\text{initial}}, R\}^*$ for optimal design can be selected from the minimum of the summation of links as follows:

$$\begin{aligned}
&\left[\left\{\sum \text{set}\right\}_{(i)}\right] = S_{\text{initial}_{(i)}} + R_{(i)},\\
&i = 1, 2, 3, \ldots\ ,\\
&\{S_{\text{initial}} + R\}^*_{(i)} = \min\left(\left[\left\{\sum \text{set}\right\}_{(i)}\right]\right);\\
&L_{\text{gen}} = \{S_{\text{initial}}, R\}^* \cup L_{\text{al}}.
\end{aligned} \tag{24}$$

Finally, L_{gen} can be composed from the lengths of L_{al} in Eq. (21).

For example, if L_{al} is randomly determined according to the genetic algorithm (an example is listed in Table IV), the length of the R-link can be expressed as shown in Fig. 9. The "proper initial posture

https://doi.org/10.1017/S0263574714001453 Published online by Cambridge University Press

Table IV. Example set of link parameters, L_{al}, from the SGA, where $\lambda = 4.9916$ rad.

l_{tb}	77.5591 mm	l_{pt}	217.4803 mm
l_{cptl}	72.8346 mm	l_{ptl}	95.9843 mm
l_{cpa}	57.9528 mm	l_{fm}	370.0787 mm

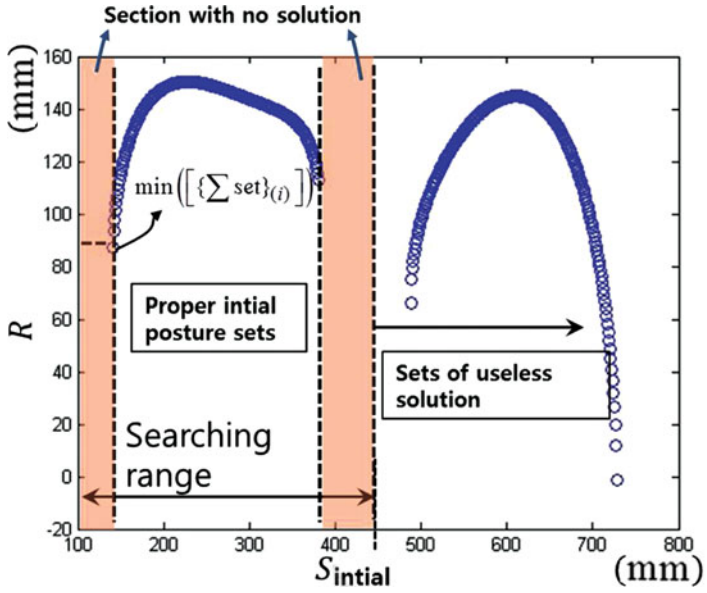

Fig. 9. (Colour online) Example of the searching process to find sets of R and S_{initial}.

sets" in Fig. 9 are those that are feasible and secured within the increment boundary condition ($S_{\text{initial}} < 465.67$ mm), which was determined from Eq. (23). When the initial condition of the searching range was set to 100 mm, S_{initial} could be determined for 141 mm, and consequently $R = 87.0633$ mm according to Eqs. (22) and (24), as shown in Fig. 9. It should be noted that R_{UC} in Fig. 8 is too short to properly connect links and there are no solutions in Fig. 9, while R_{useless} in Fig. 8 causes too large lengths of S_{initial} as shown in Fig. 9 and it is not adequate for real implementations.

4.3.3. Range of motion and power constraints (SP). Equation (25) indicates that the angle range should be larger than 50° and the angular velocity should be less than 1.35 rad/s, and that the torque should be less than 35 N m for knee angles in the range 0° –20° . The desired specifications were selected for stance-phase support of a patient with a body weight of 73 kg and a height of 174 cm, and for a gait velocity of 1.12 m/s.[26]

$$\begin{aligned}
\text{SP} &= \sum_{i=1}^{3} 10^3 \left(g_{q+}^{(i)}\right) \\
g_q^{(1)} &= 1 - \frac{\max(\theta_c)}{50^\circ}, \\
g_q^{(2)} &= 1 - \frac{\min(\dot{\theta}_c)}{1.35\,\text{rad/s}} (0^\circ \le \theta_c \le 20^\circ), \\
g_q^{(3)} &= 1 - \frac{\min(T)}{35\,\text{Nm}} (0^\circ \le \theta_c \le 20^\circ).
\end{aligned} \tag{25}$$

4.3.4. Geometric constraints (GP). To guarantee feasible solutions, a geometry penalty was applied to avoid singular configurations and unfeasible mechanism by non-convex shape, satisfying possible contact conditions. The following constraints ensure the $\overrightarrow{\text{p}_2}$ position vector is located in the triangular

https://doi.org/10.1017/S0263574714001453 Published online by Cambridge University Press

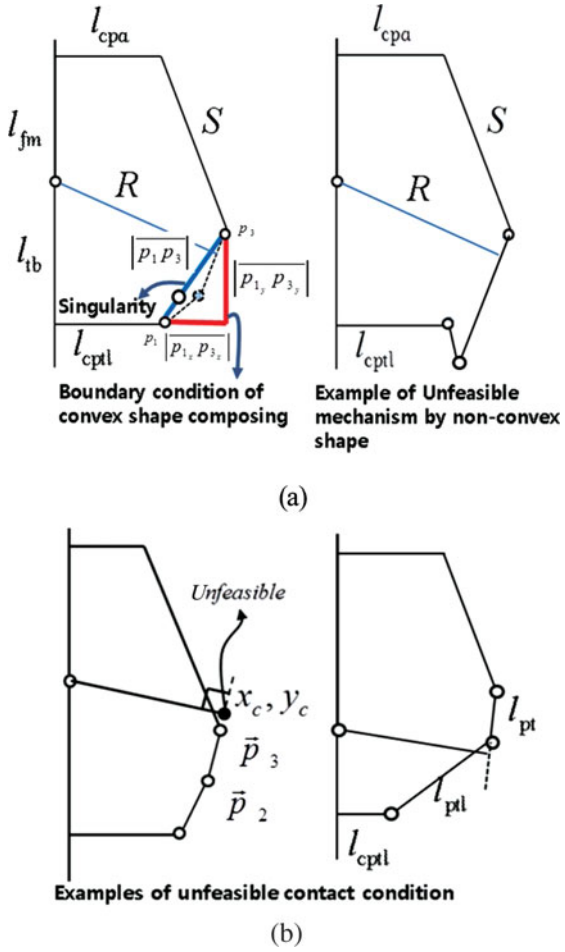

Fig. 10. (Colour online) Geometrical constraints: (a) Singular and non-convex shape avoidance condition; (b) unfeasible mechanical contact condition.

area shown in Fig. 10(a) so that the knee device can avoid singular configurations:

$$\mathrm{GP} = \sum_{i=4}^{10} 10^7 \left(g_{q+}^{(i)}\right)$$

$$\begin{cases} g_q^{(4)} = p_{3_y} - l_{\mathrm{tb}}, \quad g_q^{(5)} = l_{\mathrm{cptl}} - p_{3_x} \\ g_q^{(6)} = l_{\mathrm{cptl}} - \left|\overrightarrow{p_{1_y} p_{3_y}}\right|, \quad g_q^{(7)} = l_{\mathrm{ptl}} - \left|\overrightarrow{p_{1_x} p_{3_x}}\right|. \\ g_q^{(8)} = \left|\overrightarrow{p_1 p_3}\right| < \left(l_{\mathrm{cptl}} + l_{\mathrm{ptl}}\right) \end{cases} \tag{26}$$

The following constraint guarantees feasible solutions for mechanical contact:

$$\begin{cases} g_q^{(9)} = p_2 \vec{i} < x_c \vec{i} < p_3 \vec{i} \\ g_q^{(10)} = p_2 \vec{j} < y_c \vec{j} < p_3 \vec{j} \end{cases} \tag{27}$$

The unfeasible contact conditions are shown in Fig. 10(b).

https://doi.org/10.1017/S0263574714001453 Published online by Cambridge University Press

Table V. Results of the optimization process.

	l_{tb} (mm)	l_{cptl} (mm)	l_{cqa} (mm)	l_{pt} (mm)
Initial	248	65	110	217
Optimized	257.52	21.61	38.83	145.99
	l_{ptl} (mm)	l_{fm} (mm)	$\dot{S}$ (mm/s)	F_s (*N*)
Initial	175.87	419	320	218.8
Optimized	169.30	145.09	106.36	374.71

4.4. Parameter encoding

The genetic operator and fitness were calculated based on binary strings, and the solution space was based on variables such as link lengths, actuator stroke velocity and force. The range of valid solutions, including Q, was transformed to natural number variables called chromosomes in the coding space, where q_i is the element of Q that is initialized in the range of the valid solution, the binary string s_i is calculated by binary encoding of q_i, and the length of chromosome l_i is calculated as follows:

$$\begin{aligned} &l_i \geq \log_2 \left[10^{d_i} \left(\left| x_i^{(U)} \right| - \left| x_i^{(L)} \right| \right) + 1 \right], \\ &x_i = q_i \text{ or } h_i, \end{aligned} \tag{28}$$

where d_i is the digital resolution. To carry out the optimization using a genetic operator, we must initialize the variables. This group of variables, $P(k)$, was defined as the set of N-tuple at the kth generation, i.e.,

$$P(k) = [s_1(k), \quad s_2(k), \ldots, \quad s_N(k)] \ , \tag{29}$$

Where $s_i(k)$ is the ith set of system variables (i.e., chromosomes) and N is the size of the group.

The initial group $P(0)$ was created using a random number generator. The total number of variables was 2000 and the number of chromosomes created by the crossover was $P_cN = 85$. The number of mutations in each generation was $P_mNl = 100$. The multi-objective function satisfies the desired constraints for feasible solutions and minimizes the mass of the device via the optimization process, as shown in Fig. 11.

4.5. Optimization results

Table V shows the optimization results using the SGA process. These satisfy all the constraints in Eqs. (11)–(13). The relative size of the kinematic models of the initial design and optimal design are compared in Fig. 12. The initial design parameters were selected by trials and errors and satisfying Eqs. (8) and (21) and (25)–(27) for kinematic feasibility, boundary of the linkage lengths, the specification penalty (SP), and the geometrical penalty (GP) constraints, respectively. The slight variations of the initial values did not change the final results of Table V. For initial value design for optimization convergence, we suggested the initial posture selection scheme explained in Section 4.3.2 since the initial values in Table I did not converge due to many design parameters of the proposed kinematic device. The initial posture selection scheme could reduce eight design parameters into six design parameters with the minimum link lengths (the R-link) as shown in Fig. 11 and it finally allowed the SGA algorithm to converge the initial values in Table I into the optimization results in Table V. The relative size of the kinematic models of the initial design and optimal design are compared in Fig. 12. The kinematic parameters from the optimization also satisfy the required actuation performance, as shown in Fig. 13.

In the initial design, the summation of the link lengths, including the initial displacement of the actuator and the radius of circular structure, was 1768.87 mm. The summation of the link lengths of the optimal design was 930.45 mm, which represents a reduction of 47.4%. The actuator power that is equal to force $\times$ velocity was also reduced to 40 W, which is a 43% reduction of the initial motor power. It should be noted that the resultant maximum power of 40 W from the optimization is much less than the 160 W of Robonee.[9] In addition, the offset of the linear actuator shown in Fig. 13(a) was reduced to $S = 100$ mm, which provides greater ease of implementation. The velocity and torque

https://doi.org/10.1017/S0263574714001453 Published online by Cambridge University Press

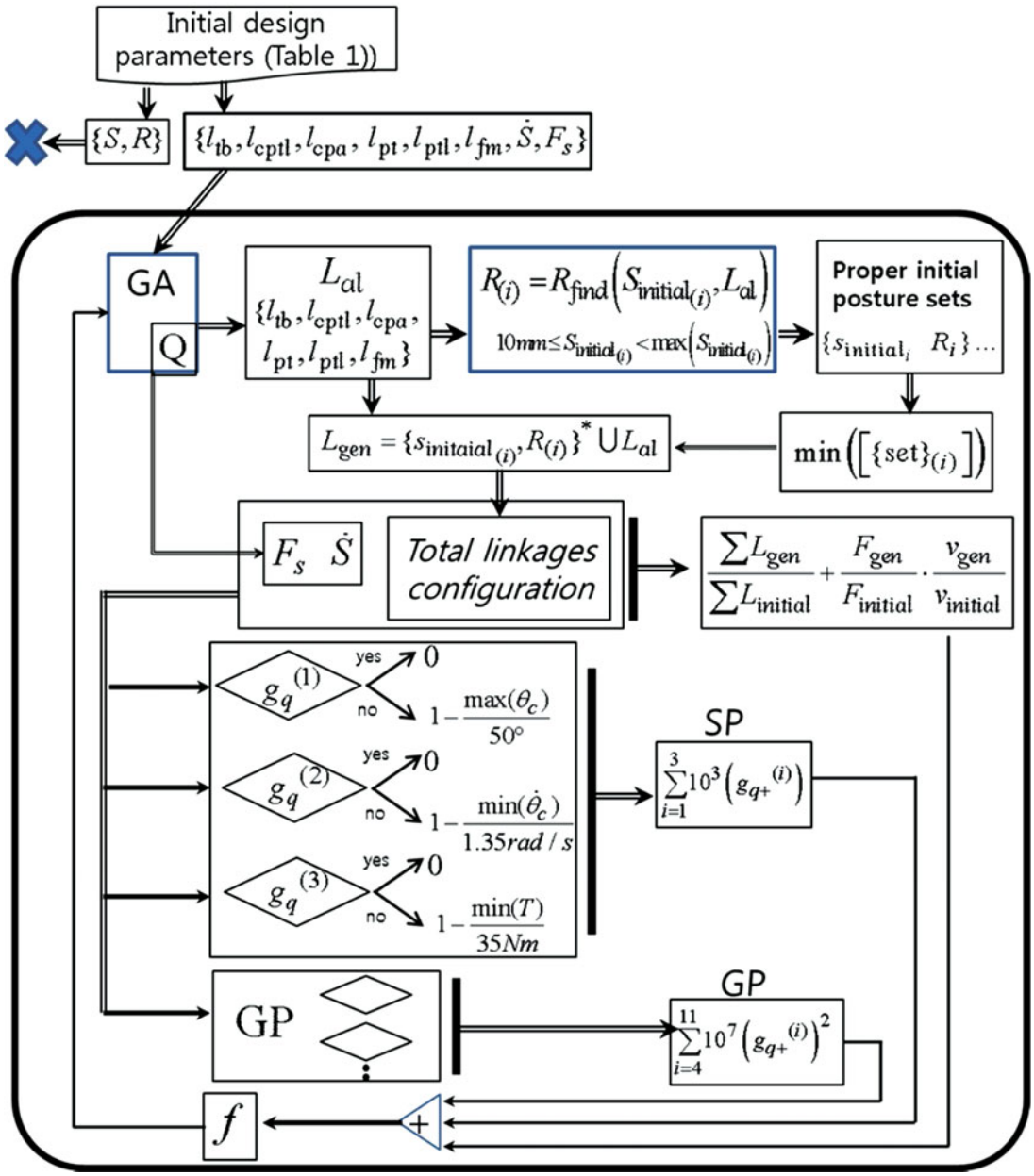

Fig. 11. (Colour online) Flow chart showing the optimization process.

of the optimized design can also satisfy the requirements over a wider range of knee angles than the initial design, as shown in Figs. 13(b) and 13(c). Furthermore, the actuator stroke velocity($\dot{S}$)becomes smaller to 106 mm/s from 320 mm/s, which can be achieved through a general linear actuator.

4.6. Prototype

A prototype device based on the optimization is shown in Fig. 1. The prototype is composed of the proposed five bar linkage system (1.9 kg), a RGO structure (3.2 kg), and a linear actuator (0.8 kg) as shown in Fig. 1. The Roboknee's weight[9] is 3 kg with the motor power of 164W (actuator weight: 1.13 kg), while the proposed system weighs 5.9 kg with the motor power of 40 W (actuator weight: 0.8 kg). It should be noted that the Roboknee aims to provide power augmentation of a healthy person with partial weight support, while the proposed system has been designed to provide gait rehabilitation functionalities of a stroke patient with full support of the patient's weight during stance phase.

https://doi.org/10.1017/S0263574714001453 Published online by Cambridge University Press

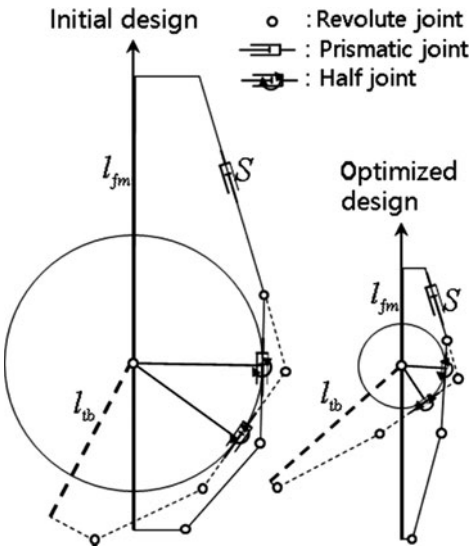

Fig. 12. Relative size of the initial and optimized systems.

Tests were carried out on a healthy subject to determine whether the mechanism could be switched from passive to active modes in response to different gait conditions of the walker. The different postures used can be seen in the snapshots shown in Fig. 14. The subject was able to freely move his knee through a knee angle range of 0° –30° when the length of the actuator was 141.279 mm, and he could stand under contact conditions with a knee angle of 30° . The experiments demonstrated that the subject could move freely during non-contact conditions, and was supported during contact conditions as shown by Figs. 13(a) and 14. Furthermore, the contact and non-contact conditions could be switched. The support was noticed by the subject, and the device was able to provide moments to counteract the motion of the user when stumbling occurred. These tests only show that the proposed working concepts of the prototype could be achieved kinematically with a fixed actuator displacement and further studies with a feedback control will be performed with varying displacements of the actuator.

5. Discussion

Robotic wearable assistive devices or exoskeletons are highly desirable and can provide movement therapy for patients with lower limb problems. However, current wearable exoskeletons cannot detect the patient's movement intentions, and so the enhancement of overground gait is limited. The device described here provides two modes of operation that can be switched based on the motion of the patient. The device can function as both a powered exoskeleton and a passive orthosis. Similar to SCKAFOs,[19] our device utilizes a locking mechanism to provide the necessary gait support while bearing weight. However, since our device is active, it can provide more functionality that existing SCKAFOs. Furthermore, we were able to reduce the mass of the device and employ a smaller actuator, which can overcome the limitations of some exoskeleton approaches that lead to large bulky pieces of equipment. The design features for the device can be summarized as follows:

- Locking the knee flexion at a desired knee angle rather than just at the full knee extension, enabling the user to ascend or descend stairs, to stand with a flexed knee, and to stabilize after stumbling;
- Unlocking the knee at any desired knee angle, regardless of the braced limb loading;
- Assisting knee extension at any desired knee angle during stance;
- Minimal device weight and motor power; and
- Switching to stance–swing mode without requiring a knee extension moment to unload the joint.

The device may allow efficient gait training modes in portable environments by providing low impedance for voluntary motion and high impedance during weight-bearing periods, as well as assisting knee extension at any desired knee angle.

https://doi.org/10.1017/S0263574714001453 Published online by Cambridge University Press

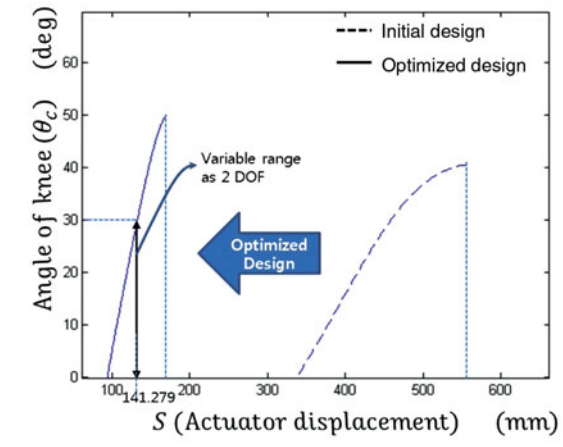

(a)

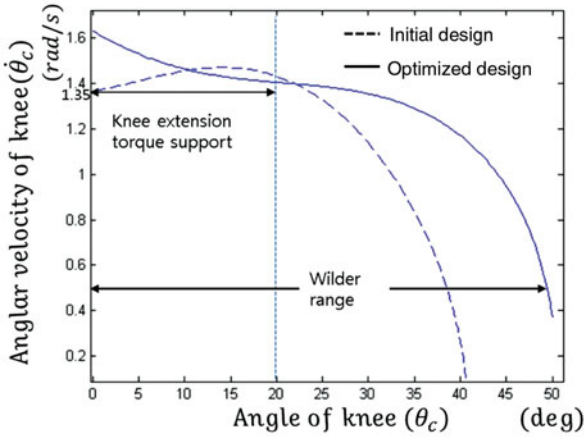

(b)

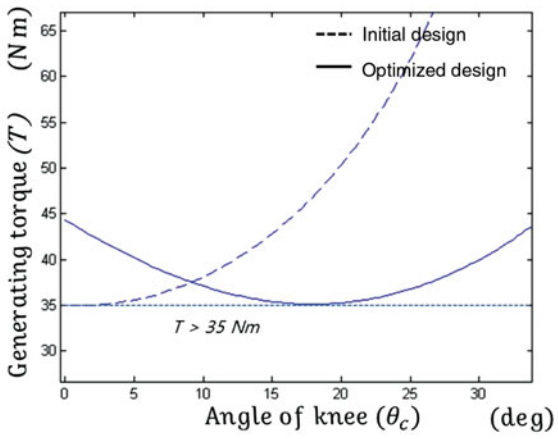

(c)

Fig. 13. (Colour online) Performance comparisons between the initial and optimized designs: (a) knee angle range with respect to actuator displacement; (b) maximum achievable knee angular velocity; (c) maximum achievable knee torque.

https://doi.org/10.1017/S0263574714001453 Published online by Cambridge University Press

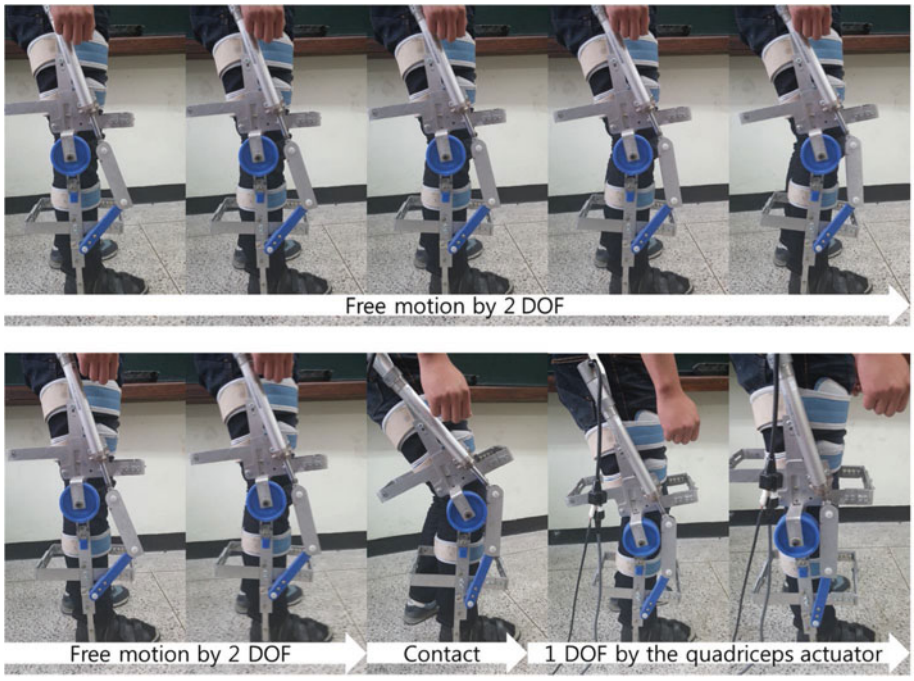

Fig. 14. (Colour online) Snapshots of the working concepts using the proposed prototype: **Free motion by 2 DOF:** if the user maintains a standing state with the actuator displacement of 141.279 mm, the proposed system becomes the five-bar linkage (2 DOF) at any angles smaller than 30° as shown in Fig. 13. The user can move his knee joint freely in flexion direction because the contact condition is not satisfied. The knee joint can have the variable angle range of 30° . **Contact:** If the displacement of the quadriceps actuator is fixed to 141.279 mm, the contact condition between the patella link and the circular structure becomes active at the knee joint of 30° . In this situation, the system's kinematic state has been changed from the five-bar linkage (2 DOF) into the six-bar linkage (1 DOF) and the user can get assistive supports from the quadriceps actuator. **1 DOF by the quadriceps actuator:** If the displacement of the actuator has been changed from 141.279 mm to 0 mm under the contact condition, the knee joint angle moves from 30° to 0° . The quadriceps actuator can support the user's knee joint at this stage.

Since stroke patients may suffer from lower muscle problems, making it difficult for them to wear a heavy exoskeleton device, a lightweight device is highly desirable. Minimizing the power of the actuator will significantly affect the mass of the resulting device. Similarly, the link lengths also contribute to the mass of the exoskeleton. A number of kinematic optimization schemes exist, including workspace optimization[23,27] and isotropy optimization;[28] however, few efforts to kinematically optimize the mass of a device have been made. We have used a technique that can reduce size of the actuator and link lengths while maintaining all necessary performance requirements, providing gait assistance and avoiding singularities. This optimization scheme may be helpful to other exoskeletons and robotic orthotic devices.

Sensorimotor techniques have been applied to help rehabilitate stroke patients.[29–31] Neuroplasticity has been recently introduced, making task-oriented training an important aspect of recovery.[32,33] Following a stroke, weakness, spasticity, and synergy may occur, which can lead to muscle contraction and shrinking of muscular fibers. Traditionally, abnormal gait patterns appear during the initial stages of recovery from a stroke; these must be minimized and controlled. Knee orthoses can be used in patients with uncontrolled knee joints to support their weight, and has been applied selectively to a limited number of patients that did not recover control of the knee joint. The robotic knee device reported here can be used to aid recovery and maintain a normal gait. It may be particularly useful as it can allow free motion of the lower limb while supporting the body weight. For stroke patients, it may help to control abnormal gait patterns during the initial recovery stage, aid sensorimotor recovery, and motivate a patient by providing support for overground walking.

https://doi.org/10.1017/S0263574714001453 Published online by Cambridge University Press

6. Conclusion

We have described the design of a novel robotic knee device with a geared five-bar linkage that allows the device to use a compact and lightweight actuator to provide support during gait training while enabling a patient to move freely within a desired range of motion. The device requires additional linkages compared to a simple four-bar mechanism. We used SGA to minimize the sum of the link lengths and the motor power, which reduced the weight of the device. To find a feasible parameter set, kinematic constraints were applied in the SGA process. The optimization scheme reduced the total length of the links and the required motor power by almost a half compared with the original design. The optimization scheme may be applied to reduce the total weight of many multi-linkages systems while maintaining functionality.

We expect the device to provide an improved rehabilitation mode for stroke patients, allowing safe, self-motivated, overground walking by providing support if the patient stumbles. For clinical applications, we plan to reduce the system's weight until less than 4.2–4.5 kg through simpler frame structure, structural design, and light-weight material as well as replacing the RGO structure by a light-weight commercial knee brace. In the future, a controller will be implemented and clinical trials will be carried out to determine the effectiveness of the device.

Acknowledgments

This work was supported by the National Research Foundation Korea (NRF) funded by the Ministry of Education, Science and Technology (2012R1A2A2A01047344, 2012-0009524, 2011-00313832010).
Min-Kyun Oh (solioh21@hanmail.net) contributed equally to this work as a corresponding author.

References

1. G. B. Prange, M. J. Jannink, G. G. Groothuis-Oudshoorn, H. J. Hermens, M. J. Ijzerman, "Systematic review of the effect of robot-aided therapy on recovery of the hemiparetic arm after stroke," *J. Rehabil. Res. Dev.* **43**(2), 171–184 (2006).
2. G. Dong-Yu, "Acute phase of stroke rehabilitation," *The Annual Fall Meeting of the Korean Stroke Society* **10**, 39–40 (2005).
3. J. Yoon, B. Novandy, C. Yoon and K. Park, "A 6-DOF gait rehabilitation robot with upper and lower-limb connections that allows walking velocity updates on various terrains," *IEEE/ASME Trans. Mechatronics* **15**(2), 201–215 (2010).
4. A. V. Nene, H. J. Hermens and G. Zilvold, "Paraplegic locomotion: A review," *Spinal Cord* **34**(9), 507–524 (1996).
5. Available at http://www.fillauer.com/pdf/M009-RGO.pdf [Accessed 29th May 2014].
6. R. Kobetic, C. S. To, J. R. Schnellenberger, M. L. Audu and T. C. Bulea, "Development of hybrid orthosis for standing, walking, and stair climbing after spinal cord injury," *J. Rehabil. Res. Dev.* **46**(3), 447–462 (2009).
7. M. Y. Zarrugh and C. W. Radcliffe, "Simulation of swing phase dynamics in above-knee prostheses," *J. Biomech*. **9**(5), 283–292 (1976).
8. D. Jin, R. Zhang, H. O. Dimo, R. Wang and J. Zhang, "Kinematic and dynamic performance of prosthetic knee joint using six-bar mechanism," *J. Rehabil. Res. Dev.* **40**(1), 39–48 (2003).
9. J. E. Pratt, B. T. Krupp, C. J. Morse and S. H. Collins, "The RoboKnee: An Exoskeleton for Enhancing Strength and Endurance During Walking", *Proceedings of the 2004 IEEE International Conference on Robotics & Automation*, New Orleans, LA, USA (Apr. 26–May 01, 2004) pp. 2430–2435.
10. G. Colombo, M. Joerg, R. Schreier and V. Dietz, "Treadmill training of paraplegic patients using a robotic orthosis," *J. Rehabil. Res. Dev.* **37**(6), 693–700 (2000).
11. S. Mefoued, S. Mohammed and Y. Amirat, "Knee Joint Movement Assistance Through Robust Control of an Actuated Orthosis," *2011 IEEE/RSJ International Conference on Intelligent Robots and Systems*, September 25–30, San Francisco, CA, USA (2011).
12. J. Nikitczuk, B. Weinberg, P. K. Canavan and C. Mavroidis, "Active knee rehabilitation orthotic device with variable damping characteristics implemented via an electrorheological fluid," *IEEE/ASME Trans. Mechatronics* **15**(6), 952–960 (2010).
13. G. Belforte, L. Gastaldi and M. Sorli, "Pneumatic active gait orthosis," *Mechatronics* **11**, 301–323 (2001).
14. J. F. Veneman, R. Ekkelenkamp, R. Kruidhof, F. C. T. van der Helm and H. van der Kooij, "A series elastic- and Bowden-cable-based, actuation system for use as torque actuator, in exoskeleton-type robots," *Int. J. Robot. Res.* **25**(3), 261–281 (Mar. 2006).
15. M. Ackermann and F. G. Cozman, "Automatic knee flexion in lower limb orthoses," *ABCM* **31**(4), 305–311 (2009).
16. J. S. Sulzer, R. A. Roiz, M. A. Peshkin and J. L. Patton, "A highly backdrivable, lightweight knee actuator for investigating gait in stroke," *IEEE Trans. Robot.* **25**(3) 539–548 (Jun. 2009).

https://doi.org/10.1017/S0263574714001453 Published online by Cambridge University Press

17. P. W. Duncan, K. J. Sullivan, A. L. Behrman, S. P. Azen, S. S. Wu, S. E. Nadeau, B. H. Dobkin, D. K. Rose, J. K. Tilson, S. Cen, S. K. Hayden, "Body-weight–supported treadmill rehabilitation after stroke," *New England J. Med.* **364**(21), 2026–2036 (2011).
18. T. G. Hornby, D. D. Campbell, J. H. Kahn, T. Demott, J. L. Moore and H. R. Roth, "Enhanced gait-related improvements after therapist- versus robotic-assisted locomotor training in subjects with chronic stroke: a randomized controlled study," *Stroke* **39**(6), 1786–1792 (2008).
19. T. Yakimovich, E. D. Lemaire and J. Kofman, "Engineering design review of stance-control knee-ankle-foot orthoses," *J. Rehabil. Res. Dev.* **46**(2), 257–268 (2009).
20. J. R. Gage, P. A. Deluca and T. S. Renshaw, "Gait analysis: principles and applications," *J. Bone Joint Surg.* **77-A**(10), 1607–1623 (Oct. 1995).
21. I. A. De Quervain, S. R. Simon, S. Leurgans, W. S. Pease and D. McAllister, "Gait pattern in the early recovery period after stroke," *J. Bone Joint Surg.* **78**(10), 1506–1514 (1996).
22. J. H. Holland, *Adaptation in Natural and Artificial Systems* (The University of Michigan Press, Michigan, 1975).
23. Y. Hwang, J. Yoon, Christiand and J. Ryu, "The Optimum Design of a 6-DOF Parallel Manipulator with Large Orientation Workspace," *Proceedings of the 2007 IEEE International Conference on Robotics and Automation (ICRA 2007)*, Rome, Italy (Apr. 10–14, 2007), pp. 163–168.
24. Christiand and J. Yoon, "A Novel Optimal Assembly Algorithm for the Haptic Interface Application of a Virtual Maintenance System," *Proceedings of the 2008 IEEE International Conference on Robotics and Automation (ICRA 2008)*, Pasadena, USA (May 19–23, 2008), pp. 3612–3617.
25. S. Hassan and J. Yoon, "Virtual Maintenance System with a Two-Staged Ant colony Optimization Algorithm", *Proceedings of the 2011 IEEE International Conference on Robotics and Automation (ICRA2011)*, Shanghai International Conference Center, Shanghai, China (May 9–13, 2011), pp. 931–936.
26. D. A. Winter, *The Biomechanics and Motor Control of Human Gait: Normal, Elderly, and Pathological* (University of Waterloo Press, Waterloo, Canada, 1991).
27. M. Arsenault and R. Boudreau, "The synthesis of three-degree-of-freedom planar parallel mechanisms with revolute joints (3-RRR) for an optimal singularity-free workspace," *J. Robot. Syst.* **21**(5), 259–274 (2004).
28. K. Y. Tsai and K. D. Huang, "The design of isotropic 6-DOF parallel manipulators using isotropy generators," *Mech. Mach. Theory* **38**, 1199–1214 (2003).
29. B. T. Volpe, H. I. Krebs, N. Hogan, L. Edelstein, C. Diels and M. Aisen, "A novel approach to stroke rehabilitation: Robot-aided sensorimotor stimulation," *Neurology* **54**(10), 1983–1944 (2000).
30. B. T. Volpe, H. I. Krebs and N. Hogan, "Is robot-aided sensorimotor training in stroke rehabilitation a realistic option?," *Curr. Option Neurology* **14**, 745–752 (2001).
31. G. G. Fluet and J. E. Deutsch, "Virtual reality for sensorimotor rehabilitation post-stroke: The promise and current state of the field," *Curr. Phys. Med. Rehabil. Rep.* **1**, 9–20 (2013).
32. B. B. Johansson, "Brain plasticity and stroke rehabilitation: The will is lecture," *Stroke* **31**, 223–230 (2000).
33. B. Nancyl, R. Jennifer, M. Olfat, H. Monica, K. Josh, S. Amy, T. Molly and A. Gary, "Effectiveness of sensory and motor rehabilitation of the upper limb following the principles of neuroplasticity: Patients stable poststroke," *Neurorehabilitation Neural.* **17**, 176–191 (2003).

https://doi.org/10.1017/S0263574714001453 Published online by Cambridge University Press